Shearing particle monolayers: Strain-rate frequency superposition

Duyang Zang,[1,2] Dominique Langevin,[1] Bernard P. Binks,[3] and Bingbo Wei[2]
[1]*Laboratoire de Physique des Solides, Université Paris Sud and UMR CNRS 8502, 91405 Orsay, France*
[2]*Laboratory of Materials Science in Space, Northwestern Polytechnical University, Xi'an 710072, China*
[3]*Surfactant & Colloid Group, Department of Chemistry, University of Hull, Hull HU6 7RX, United Kingdom*
(Received 23 December 2008; revised manuscript received 16 July 2009; published 15 January 2010)

We report surface shear rheological measurements on monolayers of silica nanoparticles at the air-water interface. We have used the method of strain-rate frequency superposition (SRFS) to characterize the structural relaxation. We show that the rheological properties of the layers have the same universal linear and nonlinear behavior as three-dimensional soft materials. We also discuss the original healing properties of these monolayers.

DOI: 10.1103/PhysRevE.81.011604 PACS number(s): 83.60.−a, 68.03.−g, 68.65.−k, 83.80.Hj

I. INTRODUCTION

Particle monolayers at liquid interfaces were recently shown to have unique properties and to behave as soft solids in two dimensions [1–4]. When liquid droplets or air bubbles are covered by such monolayers and are distorted from their spherical shapes, they can remain nonspherical for quite a long time [5]. This could be attributed to vanishing surface tension or to other mechanical stresses created by the monolayer. Independent measurements of surface tension show that it remains finite and that these monolayers possess both compression and shear moduli [6–8]. The peculiar mechanical behavior of these interfaces probably contributes to the remarkable stability of emulsions and foams made using these particles as surface-active agents [9,10]. Particles can advantageously replace surfactants in situations where these cannot be used, for instance at high temperatures (metallic foams, oil reservoirs, etc.), hence a great number of studies is devoted to particle surface layers in order to optimize the applications.

In three dimensions, soft solids have similar responses to shear, as characterized by the complex shear modulus $G^* = G' + iG''$. At low strain amplitude γ_0, the real part of the modulus G', also called the storage modulus, is much larger than the imaginary part G'', also called the loss modulus. Above a critical strain amplitude called the yield strain amplitude γ_Y, the solid melts, G'' exhibits a maximum and then remains larger than G' afterward. Both moduli then follow power laws: $G' \sim \gamma_0^{-\nu'}$ and $G'' \sim \gamma_0^{-\nu''}$ with $\nu' \sim 2\nu''$. Figure 1 shows the typical variation of G' and G'' with γ_0 obtained with a monolayer of silica nanoparticles at the air-water interface, which looks quite similar to the variation reported for three-dimensional soft solids (hard sphere suspensions, hydrogels, emulsions, foams) [11]. The frequency (ω) dependence of the moduli recorded at constant strain amplitude is also similar for these different systems: G'' is larger than G' at low frequencies and lower at high frequencies with G'' being maximum close to the crossover point. It was recently postulated by Wyss *et al.* [11] that this behavior is associated with a common feature in three-dimensional soft solids—the decrease of the structural relaxation time with increasing strain-rate amplitude $\dot{\gamma}_0$. In normal frequency measurements, the strain is kept constant and so the strain-rate amplitude varies from data point to data point, and it becomes difficult to obtain the shear rate dependence of the structural relaxation time. By using a new type of oscillatory rheology called strain-rate frequency superposition (SRFS), where the strain-rate amplitude is fixed as the frequency is varied, Wyss *et al.* were able to isolate the response due to structural relaxation, even when it occurs at frequencies too low to be accessible with standard techniques.

II. RESULTS

In the present paper, we have applied this method to particle monolayers in order to examine if the same scaling is present in two-dimensional soft solids. We use nanoparticles of partially hydrophobic silica, the degree of hydrophobicity being characterized by the percentage x of surface SiOH groups, i.e., those not replaced by silane groups [7]. These samples are composed of near-spherical primary particles of approximately 20 nm diameter, partially fused into clusters of approximately 200 nm diameter. We will present data for $x=20\%$ (most hydrophobic), 34% and 62% (least hydrophobic), for which the contact angles θ at the air-water interface are calculated to be 40°, 120°, and 135°, respectively, corresponding to adsorption energies (from the preferred wetting phase) of 300, 1400. and 480 kT per primary particle. If we take a larger effective radius to account for the partial clusters, these energies will be even higher since they vary with

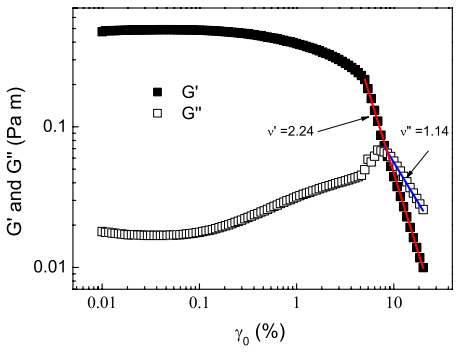

FIG. 1. (Color online) Strain amplitude sweep of a silica particle (possessing 34% SiOH) monolayer at the air-water surface. $\Gamma = 50$ mg m^{-2} and $\omega = 2$ Hz.

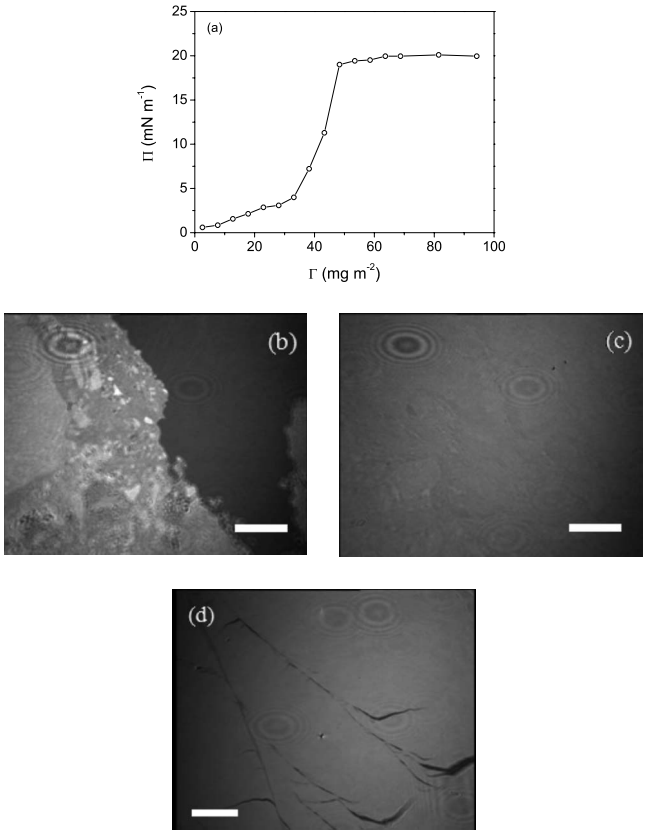

FIG. 2. Surface pressure and BAM images of the silica particle monolayer (34% SiOH) at the air-water surface (a) Surface pressure *vs* surface concentration. (b)-(d) BAM images at surface concentrations equal to (b) 20 mg m^{-2}, (c) 50 mg m^{-2} and (d) same as (c) but fractured just after the beginning of an expansion. The scale bars correspond to 1 mm.

the square of the particle radius. Provided the dispersions are sonicated for long enough in order to break the weakest clusters, the final clusters are fairly monodisperse and have approximately spherical shapes. Light scattering experiments were performed in order to characterize their size and polydispersity [12]. Upon increasing x, the hydrodynamic radius R decreases from ca. 87 nm for $x=20\%$, to 85 nm for $x=34\%$ and 72 nm for $x=62\%$. The polydispersity index $p=(\langle R^2\rangle-\langle R\rangle^2)/\langle R\rangle^2$ is 0.11, 0.2 and 0.21 for $x=20\%$, 34%, and 62%, respectively. The clusters are spherical on average (as revealed by the ratio of the hydrodynamic to gyration radius) [12].

Figure 2(a) shows the surface pressure Π measured in a Langmuir trough (Nima 601BAM, total area 500 cm^2) as a function of the surface coverage by particles Γ (mass per unit area). The particles were spread from dispersions in isopropyl alcohol, which were sonicated in order to break the large particle clusters and ensure perfect reproducibility of the surface pressure curves. Let us recall that Π is the difference between the surface tension before and after spreading. Brewster angle microscopy (BAM) images (taken with a MiniBAM, NFT-Nanofilm Technology, Göttingen) corresponding to different regions of the surface pressure curves are also shown in the figure. One sees that at low surface coverage, the surface pressure is close to zero and the surface

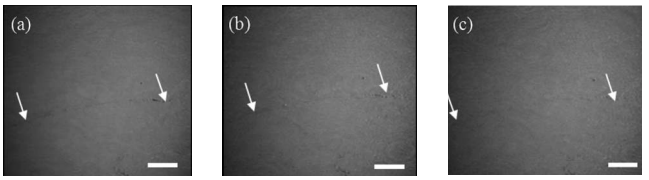

FIG. 3. BAM images of a fracture in the monolayer of particles with $x=34\%$ at a surface concentration equal to 50 mg m^{-2}, after (a) 1 s, (b) 300 s, (c) 3600 s. The fracture is no longer visible at this scale after 15 h. The scale bars correspond to 500 μm, and the arrows indicate the position of the fracture.

layer is made of disconnected patches covered by particles (b). At larger surface coverages (c), the surface pressure saturates and the layer becomes homogeneous, but can be fractured, e.g., by increasing the surface area using the barriers of the trough (d). When the layer is recompressed, the fracture heals but defects remain visible during several hours. Fractures can be also created by shearing the layer using a small needle. Again the fractures heal rapidly, but their trace remains visible during several hours (see Fig. 3). These results suggest that the monolayers are soft solids and that the relaxation times are very long. Note that particle adsorption energies are too large to allow them to desorb from the surface.

Figure 1 shows the shear moduli measured at a frequency of 2 Hz with a PAAR-Physica rheometer M 301 equipped with a bi-cone device to measure the surface shear moduli G' and G''. As expected, they are nonzero above the concentration at which the islands merge (Fig. 2). At small strain amplitude ($\gamma_0<0.1\%$), G' and G'' do not depend on strain amplitude: this is the linear régime. In this régime, the behavior is predominantly elastic: G' is about 20 times larger than G''.

At the frequency used, the yield strain amplitude γ_Y is quite high-10%-much higher than for other nanoparticles (silver) adsorbed at an oil-water interface [3]. As for three-dimensional systems, for $\Gamma=50$ mg m^{-2} the yield stress (σ_Y) varies with shear rate as: $\sigma_Y=\sigma_{Y0}+A\dot{\gamma}_0^{\mu}$, with $\sigma_{Y0}=3.07$, 2.77, and 1.15 mPa m, $A=3.3\times10^{-6}$, 5×10^{-6}, and 1×10^{-6} in SI units and $\mu=1.27$, 1.65, and 1.94 for particles with 20%, 34%, and 62% SiOH, respectively.

Since relaxation processes are quite slow in these layers, we made melting cycles in order to evaluate the time scales involved. The data are shown in Fig. 4. During the first period, the strain is increased (see upper part of figure, period labeled 1), it reaches the yield stress and the layer melts: G' decreases and G'' increases. After this first period, the strain is released rapidly, the layer solidifies back and G' increases and G'' decreases very rapidly (less than 1s), but the moduli (G' and G'') remain lower than before melting. When the strain is increased again in period 2, melting occurs and G' falls again. A third stress cycle performed during period 3 leads to the same results. In the fourth period, no strain is applied: one sees that G' increases first very quickly as in the previous cycles, then much more slowly and tends toward the initial value before the series of cycles. The characteristic time τ_0' for this increase is quite long, a few thousands of seconds. It is therefore only when the layer is allowed to

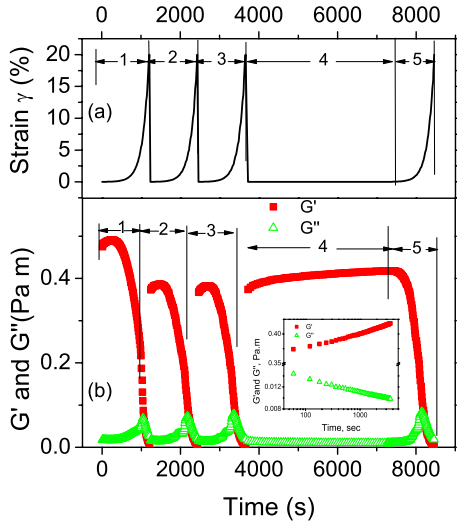

FIG. 4. (Color online) Rapid recovery and self-healing of moduli of silica particle (34% SiOH) monolayer, $\Gamma=50$ mg m^{-2}. (a) Strain amplitude as a function of time for different cycles. (b) Variation of G' and G'' in multicycle amplitude sweep. The inset graphic shows the moduli relaxation dynamics in interval 4. The numbers in the top figure correspond to the different stress cycles as explained in the text.

"heal" during long times that the initial modulus is recovered. This behavior is classical of three-dimensional soft solids. The strain amplitude dependence of the moduli after melting is also similar: $G' \sim \gamma_0^{-\nu'}$ and $G'' \sim \gamma_0^{-\nu''}$, with $\nu'=1.68$, 2.24, and 3.06 and $\nu''=0.79$, 1.14, and 1.30 for particles with 20%, 34%, and 62% SiOH, respectively (see Fig. 1 for 34%, data not shown for the other particles).

We have applied the SRFS procedure of Ref. [11] and collected a number of measurements of storage and loss moduli made keeping the strain-rate amplitude constant and found that, as for three-dimensional systems, they can be scaled onto a single curve: G'/a and G''/a versus ω/b, where a and b are functions of the shear rate only (Fig. 5). Figure 5(a) collects data for $\dot{\gamma}_0$ between 10^{-4} and 1.5 s^{-1} for the most hydrophobic silica particle monolayers (20% SiOH). The scaling is reasonably good, even at high frequency, whereas in three-dimensional systems a correction with a $\sqrt{\omega}$ dependence is needed (arising from viscous flow along randomly oriented planes [13]). Similar results were obtained with particles of different hydrophobicity at the same surface coverage and are shown in Figs. 5(c) and 5(e) (the surface pressure curves for these particles are similar to those of Fig. 2(a) [7]). As for three-dimensional systems, a is approximately constant and of order 1 whereas b varies appreciably (approximately linearly with $\dot{\gamma}_0$), see Figs. 5(b), 5(d), and 5(f). In these reduced units, the maximum of G'' for nanoparticle layers is located at $\omega/b \sim 5\times10^{-3}$ s^{-1} (7×10^{-3} s^{-1} for $x=20\%$, 5×10^{-3} s^{-1} for 34%, 10^{-3} s^{-1} for 62%).

The relaxation time (or inverse of this frequency) therefore scales as

$$\frac{1}{\tau} \approx \frac{1}{\tau_0} + K\dot{\gamma}_0^{\nu}. \quad (1)$$

At the surface coverage of 50 mg m^{-2}, $\nu \sim 0.98$, 1.08, and 1.31 for the different particles studied, $x=20\%$, 34%, and 62%, respectively [see Figs. 5(b), 5(d), and 5(f)]. This is as for three-dimensional systems for which $\nu \sim 0.9$. The amplitude K and the relaxation time at low strain increase with particle hydrophilicity; $K=4.3$, 5.1, and 9.1 (in s$^{\nu-1}$ units) and $\tau_0=1600$, 3900, and 7000 s for $x=20\%$, 34%, and 62%, respectively. It should be noted that for consistency, ν should be equal to ν'' which is indeed the case. Note that ν appears to increase slightly with particle hydrophobicity. Unfortunately, the τ_0 values for our systems are large and the frequency and amplitude ranges available with the rheometer have not allowed us to collect enough data points in the low strain rate region and to access better the saturation behavior. As a consequence, the accuracy of the determination of τ_0 is very limited. However, the quality of the fits including a finite τ_0 is definitely better. Note that the time τ_0' for the self-healing behavior in experiments such as those of Fig. 4 is of the same order of magnitude and also increases with x: more hydrophobic particle layers heal faster.

III. DISCUSSION

Let us now discuss the possible physical origin of this relaxation. The structural relaxation of colloidal systems involves rearrangements of particles relative to each other (including "escape from the cage" in a cage model). The time scale of these rearrangements is usually greatly influenced by applied shear, and described by Eq. (1). The equivalence between frequency and strain rate used in the SFRS method is based on the fact that the relaxation depends only on the amplitude of the deformation, not on its time dependence [14]. When the equivalence holds as here, the linear response at high frequency and the nonlinear response at low frequency should be governed by the same particle rearrangements.

This may seem contradictory with the behavior observed for large stresses: when the surface layer is sheared above the yield stress, it melts and may fracture at scales much larger than the particle size, as seen in the BAM images such as those of Fig. 3. The images reveal that fractures heal quickly, but that residual defects take time to disappear. This could be at the origin of the variations of the shear moduli shown in Fig. 4: the two characteristic times (fast and long) evaluated from texture evolution with BAM are comparable to those from rheology measurements, and the long recovery time τ_0' is of the same order of magnitude as τ_0. However, the presence of fractures was not demonstrated in the rheometer; furthermore, the stresses exerted to create fractures in the Langmuir trough were not controlled, and could be much larger than those exerted in the rheometer. Hence the similarities between the τ_0' and τ_0 could be a coincidence.

Let us discuss further the fracture behavior. It is at first sight strange to observe such an easy healing: if the particles were held together by van der Waals forces, these forces would be too strong to allow the layer to fracture reversibly.

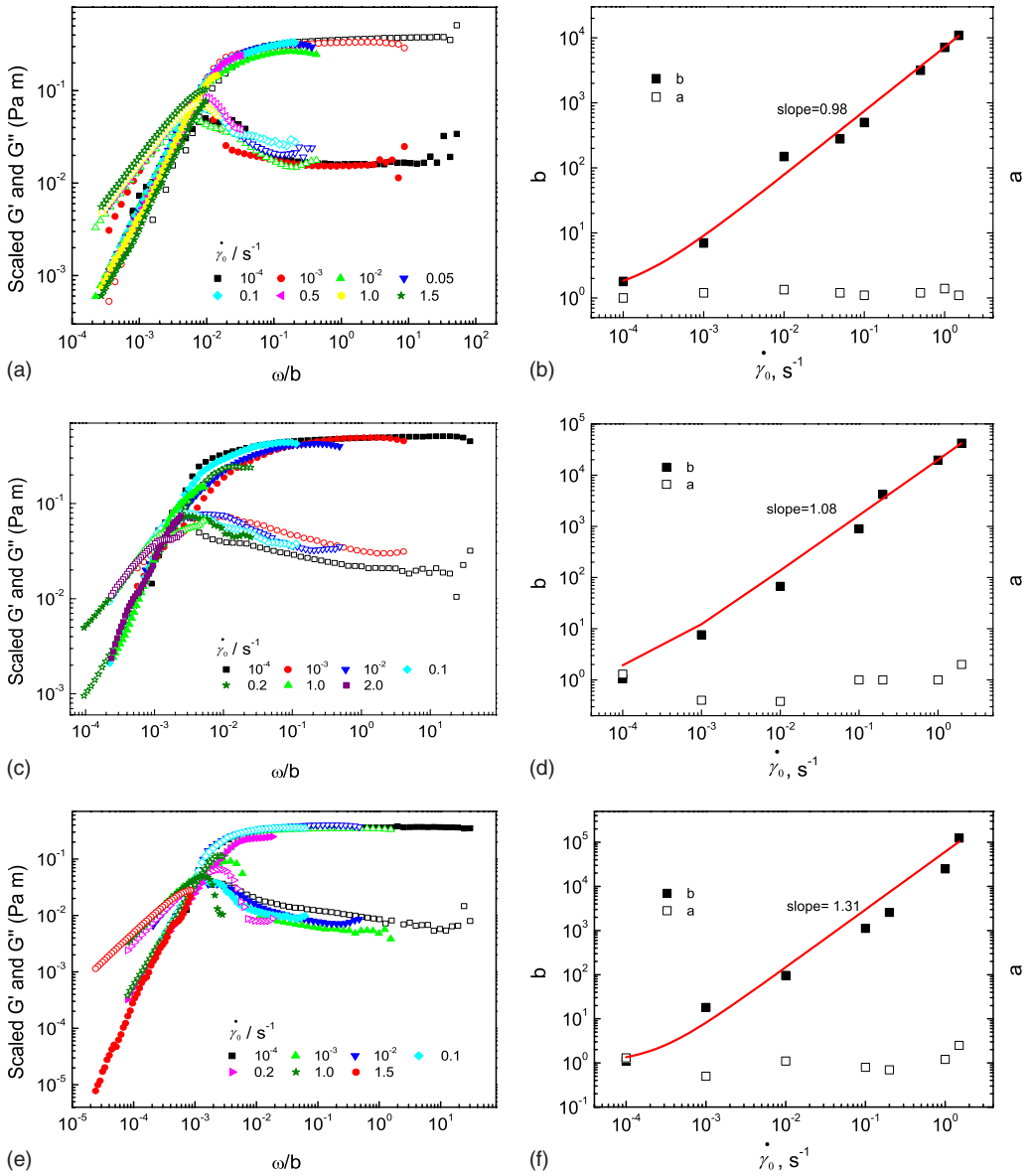

FIG. 5. (Color online) Strain rate frequency superposition measurements of monolayers with $\Gamma=50$ mg m^{-2}. Data were taken for different $\dot{\gamma}_0$ varying from 10^{-4} to 1.5 or 2.0 s^{-1}. Left curves: constant shear rate sweep measurements shifted onto a single master curve: (a) $x=20\%$, (c) $x=34\%$, (e) $x=62\%$. Right curves: corresponding amplitudes (a, right ordinate) and frequency (b, left ordinate) scaling factors vs $\dot{\gamma}_0$.

Since the surface coverage just before buckling is about 50 mg m^{-2} and the layer thickness is about 200 nm, the fraction of area covered is about 10% (the density of silica is 2 g cm^{-3}) and the distance between particles is about three times their radius, as confirmed by recent ellipsometry determinations [15]. This is a clear proof of the existence of long range repulsive forces, probably electrostatic, which for nanoparticles are of the Debye-Hückel type instead of algebraically decaying with distance for micron sized particles [16]. Even if van der Waals forces hold the primary silica particles together in the clusters, these clusters cannot approach to small distances due to the repulsive forces. Note that the clusters are rough and that it can be shown that the attractive capillary interaction at these distances is negligible [17]. If the potential is as in bulk, a combination of Debye-Hückel repulsion and van der Waals attraction, the shallow minimum could occur in the overall interaction potential at distances between particles equal to several times their diameter, explaining why particle rearrangements are easy and fractures reversible.

We find that the healing time τ_0' is smaller for the more hydrophobic particles; these particles are probably the least charged, meaning that the potential well could be deeper, hence accounting for a larger restoring force driving particle rearrangements. Let us finally mention that the typical surface coverage where the surface layers are strongly viscoelastic, but where the relaxation times are still measurable, is 50 mg m^{-2}. Above this value, the relaxation times are prohibitively long. This corresponds to an area fraction of about 10%, as discussed before. It is surprising to observe

particle jamming at this low area fraction. Note that a recent study of charged and uncharged microgel particles in bulk evidenced that jamming occurs at a lower volume fraction for the charged particles [18]. The effect seen here could have the same origin.

IV. CONCLUSIONS

In summary, we have shown that two-dimensional layers of nanoparticles form soft solids once compressed above a few tens of mg m^{-2}. The shear rheological behavior of these solids is remarkably similar to that of three-dimensional solids held by small interaction forces. The use of the SRFS method allows the determination of a characteristic relaxation time that varies approximately linearly with the inverse of the shear rate as in the three-dimensional case. When fractures are created, they are able to heal fast, a process followed by slow disappearance of defects created during the fast healing. The self-healing process observed shares some resemblance with the rheological behavior (time evolution of G' after a melting cycle, influence of hydrophobicity on the time scales), but the link between the two behaviors remains to be established.

ACKNOWLEDGMENTS

We are grateful to Wacker-Chemie (Burghausen) for the gift of the particles. We have benefited from fruitful discussions with M. Oettel and S. Dietrich.

[1] P. Cicuta, E. J. Stancik, and G. G. Fuller, Phys. Rev. Lett. **90**, 236101 (2003).
[2] H. König, R. Hund, K. Zahn, and G. Maret, Eur. Phys. J. E **18**, 287 (2005).
[3] R. Krishnaswamy, S. Majumdar, R. Ganapathy, V. V. Agarwal, A. K. Sood, and C. N. Rao, Langmuir **23**, 3084 (2007).
[4] S. Reynaert, P. Moldenaers, and J. Vermant, Phys. Chem. Chem. Phys. **9**, 6463 (2007).
[5] A. B. Subramaniam, M. Abkarian, L. Mahadevan, and H. A. Stone, Langmuir **22**, 10204 (2006).
[6] R. Aveyard, J. H. Clint, D. Nees, and N. Quirke, Langmuir **16**, 8820 (2000); R. Aveyard, J. H. Clint, D. Nees, and V. N. Paunov, *ibid.* **16**, 1969 (2000).
[7] M. Safouane, D. Langevin, and B. P. Binks, Langmuir **23**, 11546 (2007).
[8] C. Monteux, E. Jung, and G. G. Fuller, Langmuir **23**, 3975 (2007).
[9] B. P. Binks, Curr. Opin. Colloid Interface Sci. **7**, 21 (2002).
[10] A. Cervantes Martinez, E. Rio, G. Delon, A. Saint-Jalmes, D. Langevin, and B. P. Binks, Soft Matter **4**, 1531 (2008).
[11] H. M. Wyss, K. Miyazaki, J. Mattsson, Z. Hu, D. R. Reichman, and D. A. Weitz, Phys. Rev. Lett. **98**, 238303 (2007).
[12] A. Stocco, W. Drenckhan, E. Rio D. Langevin, and B. P. Binks, Soft Matter **5**, 2215 (2009).
[13] A. J. Liu, S. Ramaswamy, T. G. Mason, H. Gang, and D. A. Weitz, Phys. Rev. Lett. **76**, 3017 (1996).
[14] K. Miyazaki, H. M. Wyss, D. A. Weitz, and D. R. Reichman, Europhys. Lett. **75**, 915 (2006).
[15] D. Y. Zang, A. Stocco, D. Langevin, B. Wei, and B. P. Binks, Phys. Chem. Chem. Phys. **11**, 9522 (2009).
[16] D. Frydel, S. Dietrich, and M. Oettel, Phys. Rev. Lett. **99**, 118302 (2007); M. Oettel and S. Dietrich, Langmuir **24**, 1425 (2008).
[17] M. Oettel (private communication).
[18] S. Schmidt, T. Hellweg, and R. von Klitzing, Langmuir **24**, 12595 (2008).